AGU PUBLICATIONS

Geophysical Research Letters

RESEARCH LETTER
10.1002/2014GL062051

Key Points:
- Seasonal temperature cycle found in the subsurface warm layer around Greenland
- There is a distinctive spatial variability to the phase of the seasonal cycle
- Phase of seasonal cycle related to water's travel time from the Irminger Sea

Supporting Information:
- Readme
- Figure S1
- Movie S1

Correspondence to:
J. P. Grist,
jeremy.grist@noc.ac.uk

Citation:
Grist, J. P., et al. (2014), Seasonal variability of the warm Atlantic water layer in the vicinity of the Greenland shelf break, *Geophys. Res. Lett.*, *41*, doi:10.1002/2014GL062051.

Received 2 OCT 2014
Accepted 7 NOV 2014
Accepted article online 13 NOV 2014

Seasonal variability of the warm Atlantic water layer in the vicinity of the Greenland shelf break

Jeremy P. Grist[1], Simon A. Josey[1], Lars Boehme[2], Michael P. Meredith[3,4], Kristin L. Laidre[5], Mads Peter Heide-Jørgensen[6], Kit M. Kovacs[7], Christian Lydersen[7], Fraser J. M. Davidson[8], Garry B. Stenson[8], Mike O. Hammill[9], Robert Marsh[10], and Andrew C. Coward[1]

[1]National Oceanography Centre, University of Southampton Waterfront Campus, Southampton, UK, [2]Sea Mammal Research Unit, University of St Andrews, Scotland, UK, [3]British Antarctic Survey, High Cross, Madingley Road, Cambridge, UK, [4]Scottish Association for Marine Science, Oban, Scotland, UK, [5]Polar Science Center, Applied Physics Laboratory, University of Washington, Seattle, Washington, USA, [6]Greenland Institute of Natural Resources, Nuuk, Greenland, [7]Norwegian Polar Institute, Fram Centre, Tromsø, Norway, [8]Fisheries and Oceans Canada, St. John's, Canada, [9]Maurice Lamontage Institute, Fisheries and Ocean Canada, Mont-Joli, Canada, [10]Ocean and Earth Science, University of Southampton, National Oceanography Centre, Southampton, UK

Abstract The warmest water reaching the east and west coast of Greenland is found between 200 and 600 m. While important for melting Greenland's outlet glaciers, limited winter observations of this layer prohibit determination of its seasonality. To address this, temperature data from Argo profiling floats, a range of sources within the World Ocean Database, and unprecedented coverage from marine-mammal borne sensors have been analyzed for the period 2002–2011. A significant seasonal range in temperature (~1-2°C) is found in the warm layer, in contrast to most of the surrounding ocean. The phase of the seasonal cycle exhibits considerable spatial variability, with the warmest water found near the eastern and southwestern shelf break toward the end of the calendar year. High-resolution ocean model trajectory analysis suggests the timing of the arrival of the year's warmest water is a function of advection time from the subduction site in the Irminger Basin.

1. Introduction

The warmest water to reach the east and west coasts of Greenland is found in the 200–600 m depth range [e.g., *Fratantoni and Pickart*, 2007; *Mauritzen*, 1996]. However, harsh environmental conditions including seasonal sea-ice cover have restricted the number of year-round sub-surface observations near the Greenland shelf, making it challenging to (a) ascertain if the warm layer (hereafter WL) experiences a significant seasonal cycle, and (b) determine the characteristics of any such cycle. Nonetheless, quantifying and understanding the nature of the WL seasonal cycle are important for improving predictions of sea level rise because, temperature changes within the layer have been highlighted as a possible cause of accelerated melting of tidewater glaciers [*Holland et al.*, 2008; *Straneo et al.*, 2010; *Mortensen et al.*, 2011; *Sutherland et al.*, 2013]. In particular, the 1997 warming (relative to previous years) of the subsurface waters along the West Greenland coast has been attributed to an anomalously warm Irminger Current associated with a shift in the phase of the North Atlantic Oscillation [*Holland et al.*, 2008; *Zhu and Demirov*, 2011]. Observations of the vertical temperature structure on the West Greenland coast have been used to estimate heat content and thus the ice-melting potential of both the WL and the overlying Polar Water [*Myers and Ribergaard*, 2013]. Such studies make implicit assumptions concerning the seasonal cycle of the water masses, for example that the temperatures observed in summer are representative of the annual mean, or that the Irminger Water summer temperatures are the annual maxima [*Holland et al.*, 2008; *Myers and Ribergaard*, 2013].

In this study, the seasonal cycle of the subsurface WL is explored using in situ observations from Argo floats as well as the range of platforms collated by the World Ocean Data Base (WODB), complemented with a large number of temperature measurements taken from marine-mammal borne sensors between 2002 and 2011. A number of studies have used temperature measurements from animal-borne instruments to derive useful physical oceanographic insights. The enhanced spatiotemporal sampling enabled by the animals residing for periods in relatively restricted areas frequently yield data sets that differ radically from those obtained using conventional techniques [*Boehme et al.*, 2008a; 2008b; *Charrassin et al.*, 2008; *Meredith et al.*,

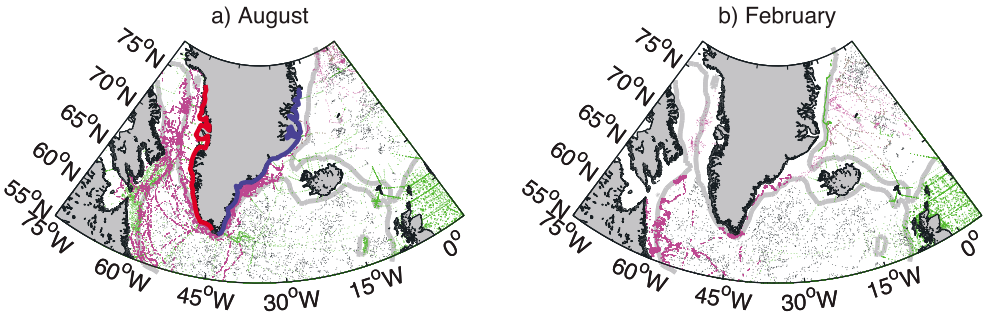

Figure 1. (a) Distribution of temperature profiles (2002–2011) from World Ocean Data Base (WODB) (green dots), Argo profiling floats (black dots), and marine mammal-borne sensors (magenta dots) used in the (a) August and (b) February objective analysis. Red and blue lines around the Greenland coast refer to the sections analyzed in Figure 3. The 600 m bathymetric contour is shown in grey. As observations in the North Sea have negligible influence on the analysis close to the Greenland coast, WODB profiles in the North Sea are excluded from number of profiles cited in section 2.

2011; *Sutherland et al*., 2013; *Roquet et al*., 2013]. Here, we combine observations from sensors deployed on different marine-mammal species deployed by US, Canadian, Greenlandic, and Norwegian research programs. The resulting improvements in spatial coverage near the Greenland shelf and in temporal coverage in the non-summer months provide a unique opportunity to explore the seasonal variability of temperature in the subsurface WL. In addition, a hindcast of an eddy-resolving ocean model is used to investigate the causes of the observed variability.

2. Data and Analysis Procedure

Observations from several different sources collected between January 2002 and December 2011 are used in our analyses (Figure 1): (i) >110,000 WODB 2013 profiles [*Boyer et al*., 2013] from various platforms including Ocean Station data, XBTs, drifting buoys, and gliders; (ii) >46,000 Delayed-Mode Quality Controlled profiles from drifting Argo floats, not duplicated in WODB; and (iii) three temperature data sets from marine-mammal borne instruments. The first marine mammal data set consists of 48,712 profiles from hooded seals, harp seals, grey seals, and beluga whales that were tagged by scientists from Fisheries and Oceans Canada at shelf sites around the Labrador and Irminger Seas between July 2003 and May 2008 [*Andersen et al*., 2009, 2013; *Bailleul et al*., 2012]. Further details, including quality control procedures, are found in *Grist et al*. [2011] and references therein. The second marine mammal data set consists of over 109,000 observations from sensors deployed on narwhals between December 2005 and March 2008 in the Baffin Bay region [*Laidre et al*., 2010]. The third source consists of 6048 profiles obtained from hooded seals tagged in the Nordic Seas by scientists from the Norwegian Polar Institute between July 2007 and April 2009 [*Isachsen et al*., 2014].

Gridded temperature estimates and associated error bars were calculated at $1 \times 1°$ resolution on standard World Ocean Atlas (WOA) levels using the objective analysis (OA) scheme and spatial correlation scales of *Boehme and Send* [2005]. For each month of the year, estimates were made at the middle of the month using a temporal decorrelation scale of 30 days and confining the source data to that from the corresponding month, the preceding month, and the following month (e.g., January, February, and March observations are the data source for the February analysis). As determining the seasonal variability was the goal of the study, the OA was conducted using data from each month irrespective of year. Interannual variability is thus neglected in the resulting estimates but reflected in the size of their errors. The source data available for August and February are shown in Figure 1. As Argo floats are confined to off-shelf areas and other WODB sources are greatly reduced in the winter, the importance of the enhanced coverage from marine mammals near the Greenland coast in non-summer months is evident. A recent gridded estimate of the mean annual temperature field used the on-shelf observations from marine-mammals borne sensors [*Grist et al*., 2011] and substantially improved the depiction of the temperature structure associated with regions boundary currents relative to the EN3 [*Ingleby and Huddleson*, 2007] and World Ocean Atlas [*Levitus et al*., 2009] gridded estimates. However, with regard to resolving the seasonal cycle, the data coverage is still incomplete in some areas. For example, in February, there are no data between 64°N and 66°N along the West Greenland coast (Figure 1b). Despite these constraints, increased winter coverage from marine mammals together with

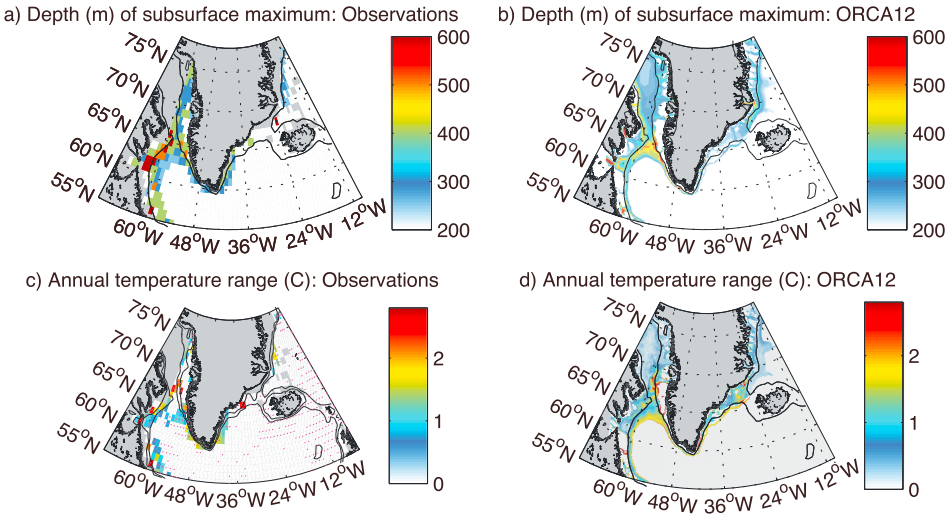

Figure 2. Depth of the subsurface temperature maximum (m) from (a) the 10 year (2002–2011) mean of the observational analysis and (b) 10 year mean of the ORCA12 global ocean only model (2001–2010). Areas with the temperature maximum near the surface (i.e., less than 200 m depth) are shown as white. (c) Observational and (d) ORCA12 analysis showing locations, where, at the depths of the subsurface maximum in Figures 2a and 2c, respectively, a seasonal cycle is detected. Here a seasonal cycle is considered not detected (white cells) where the annual temperature range is less than the sum of the errors (or standard deviation in the case of the model) of the coldest and warmest months. In Figures 2a and 2c grey cells denote areas where observations at the relevant level were absent for at least 5 months of the year. In all panels the 600 m isobath is shown (black line); additionally, the 300 m isobath is shown in Figure 2c. The magenta dots in Figure 2c denote the areas where an annual cycle is detected at the fixed subsurface level of 300 m.

an OA scheme that accounts for the stronger spatial correlation along topographically steered currents [*Boehme and Send*, 2005] allows for an improved description of the seasonal cycle around Greenland.

Observational analysis is complemented by an examination of the 2001–2010 section of the 1978–2010 hindcast from the 1/12th degree NEMO ocean model [*Madec*, 2008]. The simulation, which is hindcast ORCA0083-N001 in the DRAKKAR data set of simulations [*Barnier et al*., 2006; *DRAKKAR Group*, 2007], is referred to as ORCA12 in this paper. The higher resolution "eddy-resolving" simulation is utilized for a more realistic depiction of boundary currents [e.g., *Hecht and Smith*, 2013]. Further details of ORCA12 are documented in *Duchez et al*. [2014]. ARIANE software [*Blanke and Raynaud*, 1997] is used to calculate water particle trajectories from ORCA12 in a manner similar to that reported by *Jutzeler et al*. [2014].

3. Results

The depth of the maximum annual mean temperature is shown in Figure 2a. Over most of the domain, the temperature maximum is at the surface or within the top 200 m (white in Figure 2a). However, a distinctive feature of the Greenland, Baffin Bay, and Labrador coast regions is the existence of a vertical temperature maximum between 200 and 600 m, below the cooler fresh surface boundary current [e.g., *Tang et al*., 2004; *Fratantoni and Pickart*, 2007 and supporting information Figure S1]. The same diagnostic calculated for the 10 year mean of ORCA12 shows similar characteristics but emphasizes the small horizontal scale associated with the sub-surface temperature maximum (Figure 2b). In Figures 2c and 2d seasonal ranges in temperature at the depth of the subsurface maxima in Figures 2a and 2b, respectively, are plotted. The magnitude is shown if, in the case of the observations, it exceeds the sum of the error associated with the coolest and warmest months and in the case of the model analysis, if it exceeds the sum of the interannual standard deviations of the coolest and warmest months. Along the Greenland shelf break, an annual cycle is detected in most of the areas where there is a subsurface maximum. The seasonal range in temperature is of the order 1–2°C. The locations at which a seasonal cycle is observed at the fixed level of 300 m are shown as magenta dots in Figure 2c to provide an indication of how common it is for there to be a detectable seasonal cycle at the depth of the WL. It is possible to detect a seasonal cycle near the shelf regions of Greenland, Baffin Bay,

and Labrador. However, the seasonal variation in the subsurface temperature maxima near the Greenland shelf is not observed in much of the neighboring ocean at the same depth (Figure 2c).

We now examine if the phase of the seasonal cycle maximum is constant around the western and eastern shelf. Figures 3a and 3c show the seasonal temperature cycle of the WL around both the East and West Greenland shelf. Specifically, it shows the difference in observed monthly temperature from the annual mean temperature for the depths of 300 and 400 m, respectively. This is shown for each latitude band around the east and west coast of Greenland (where the grid cell chosen from each latitude is the one closest to the coast at that depth). It is clear that substantial spatial variability exists in the timing of the seasonal maximum. On the east coast, and south of 65° N on the west coast, the phase of the annual cycle appears to be relatively constant, with the temperature maximum occurring between September and December and the minimum occurring between February and June. Conversely, the northern region of the west coast exhibits a different phase. Typically, north of Davis Strait (65°N) the maximum occurs later (that is February or March), and the coolest months are between August and January. Although there appears to be little difference between the nature of the seasonal cycle at 300 and 400 m (Figures 3a and 3c), the signal is slightly less robust at 400 m. This is to be expected as the amount of available data diminishes with depth. The caveat to our analysis is that, while our data coverage is greatly improved, some areas are particularly sparsely covered and only have data from a single year. In such regions the error (which we associate with interannual variability) will be an underestimate; hence, it would be premature to assign temperature changes to purely seasonal as opposed to interannual variability, echoing the findings of previous studies [e.g., *Straneo et al*., 2012]. Nonetheless, there remains strong evidence for considerable spatial variability in the phase of the WL annual cycle, and this interpretation is supported by analysis of numerical model output (see below). In particular, the annual temperature maximum appears to occur later in the northern section of the west coast than at locations along the south-west and eastern coasts. An implication of this finding is that at many locations along the shelf, the warm layer often has its highest temperature during winter months when conventional (i.e., not from marine mammals) observations are few in number.

The observational analysis documented in Figures 3a and 3c has been repeated for ORCA12 (Figures 3b and 3d). The model analysis shows a similar magnitude in the range of the annual cycle. Like the observations, the peak month occurs between August and November on the east coast and south of 65°N on the west coast, with a later peak to the north on the west coast. The model's higher resolution and complete fields are better able to depict a gradual northward propagation of the peak month along the west coast from October at 61°N to May at 75°N. The annual progression of the warmest waters around at the Greenland shelf break is further illustrated dynamically in the supporting information.

An indication of the significance of the seasonal cycle is provided in Figure 3e, which shows the ratio of the seasonal range in temperature compared to the sum of the error of the warmest and coolest months for the observational analysis. For the model analysis the ratio of the seasonal range to the sum of the interannual standard deviations of the coolest and warmest month is used. The strongest seasonal signal (relative to the error range or interannual variability) is found in south-east Greenland. This signal reduces with increasing latitude along the west coast. Along the east coast north of the Denmark Strait the strength of the seasonal cycle diminishes markedly, to the point where it is about half of the error range or interannual variability in the observations and model, respectively.

The seasonal cycle and its northward propagation on the west coast are more evident in the model north of the Davis Strait at 300 m than at 400 m (Figures 3b and 3d). The suggestion is that there is a surface influence on the annual cycle in this region that is less evident on other parts of the coast. This is consistent with a large seasonal range in both surface salinity and temperature in the region associated with the seasonal advance and retreat of sea ice. An additional surface influence on the seasonal cycle in this region may also be important in producing a larger annual cycle in the vicinity of the Davis Strait, which is evident in both observations (Figure 2c, Figures 3a and 3c) and the model (Figures 2d and 3b).

To elucidate the cause of the spatial variability in the annual cycle, in particular for the south-east and west coast of Greenland where the warmest temperatures occur in winter, we conducted a particle trajectory analysis using ARIANE tracking software [*Blanke and Raynaud*, 1997]. For this, we seeded the model with particles in the subsurface temperature maxima (200–600 m) in the Irminger Basin (Figure 4a), a location close to that at which Atlantic Water at the surface descends to become separated from the direct influence of solar

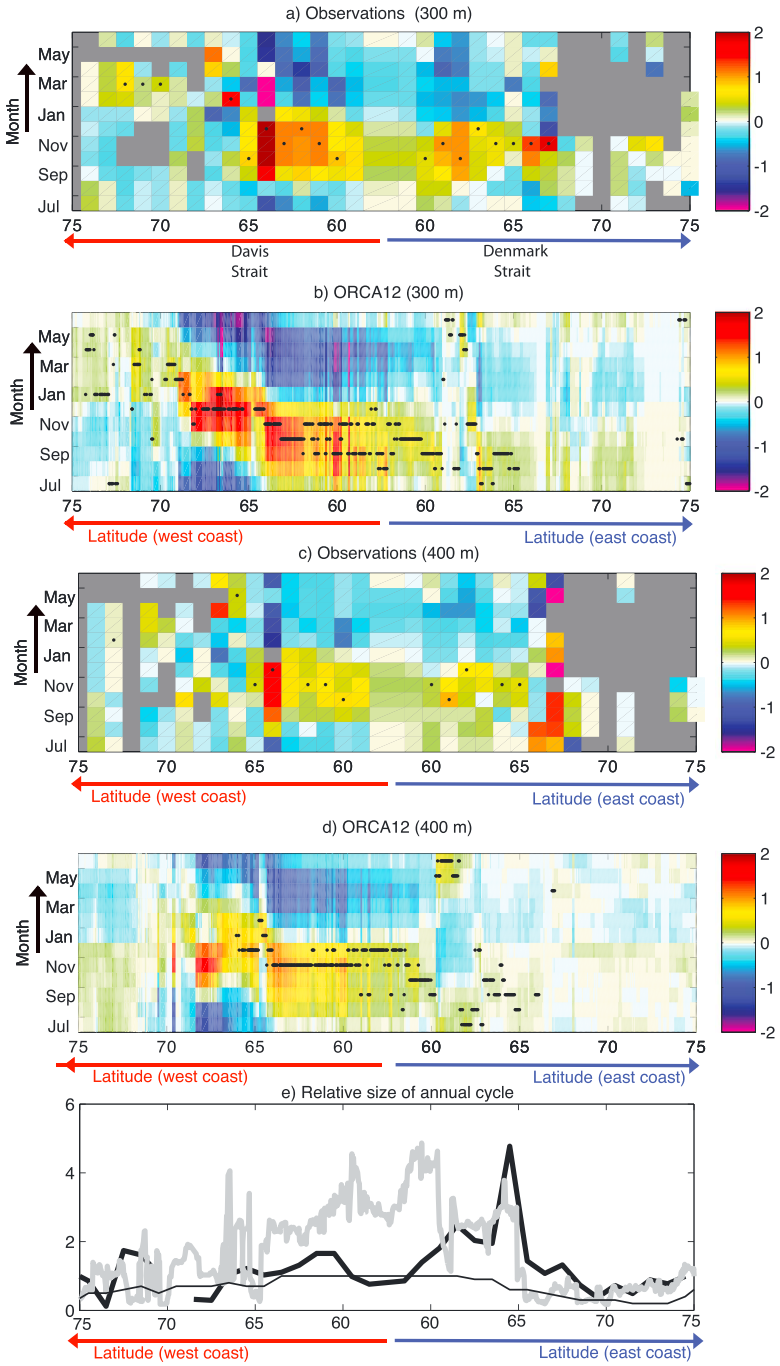

Figure 3. Hovmoller plot of the 2002–2011 mean observed seasonal cycle (shown as the anomaly from the annual mean) of the temperature at (a) 300 m and (c) 400 m along the Greenland coast. The left-hand side of the *x* axis shows the progression south from 75°N on West Greenland coast to the southern tip near 59°N, and the right-hand side shows the northward progression along the east coast to 75°N. Grey cells denote missing data, defined as being a month during which no data were collected within 100 m vertical extent and a 1 degree radius (this is decreased to 0.5 degree for the Denmark Strait because of its greater spatial variability). (b) and (d) Same as Figures 3a and 3b but for 2001–2010 from the ORCA12 ocean model. Where the seasonal amplitude is greater than the error range in Figure 3a or the standard deviation of interannual variability in Figure 3b, the warmest month is denoted by a black dot. (e) Ratio of the seasonal range (warmest month minus coolest month) to the sum of the errors at the warmest and coolest months for the observational analysis in Figure 3a (black line). Grey line is the equivalent model calculation where instead of the sum of the errors, the sum of the interannual standard deviation from the coolest and warmest months are used. The thin black line shows the fraction of the number of calendar years between 2002 and 2011 for which each grid point has an observation within 1° of latitude and longitude and 100 m depth.

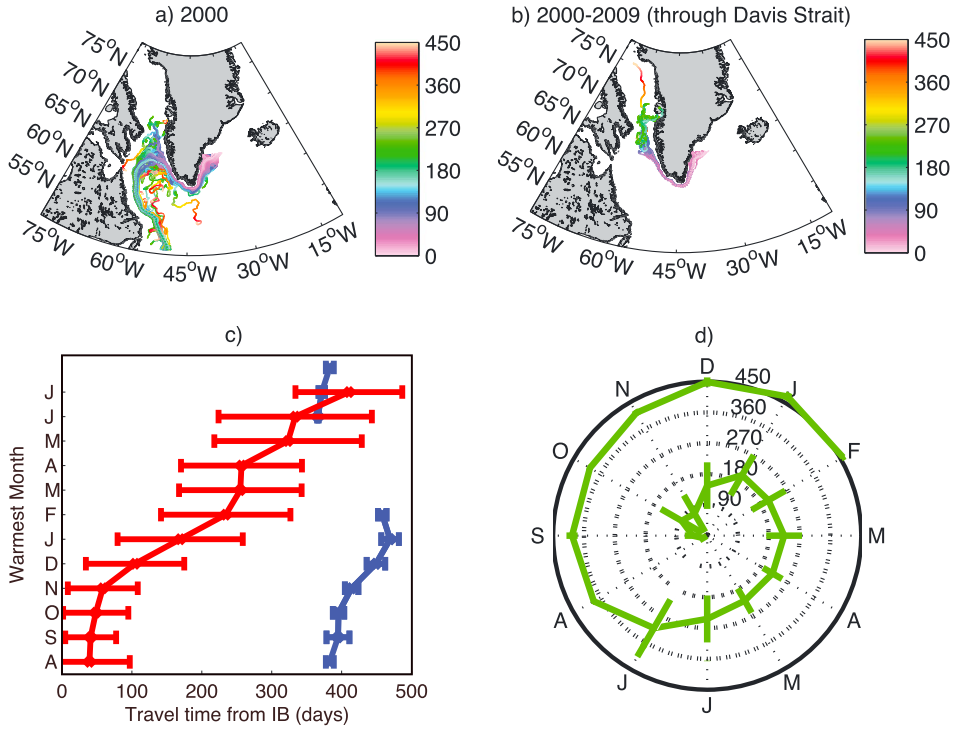

Figure 4. (a) Trajectories of particles seeded between 200 and 600 m within the warm layer off the east Greenland coast on 2 September 2000 in ORCA12. Trajectories are color coded to indicate travel time in days from release point. (b) Same as Figure 4a, and repeated for years 2001–2009 and only showing the trajectories that pass north through the Davis Strait. (c) Figure showing the relationship between the mean particle travel time from the Irminger Basin (IB) in days (error bars are standard deviation) at a particular location and the month of the annual temperature maxima at that location. Blue line denotes particles trajectories north of 72°N on the west coast, which are about 12 months later than initial trajectories. Red lines are trajectories from all other trajectories. (d) Same as Figure 4c but only using trajectories that passed through Davis Strait with the data combined together in a continuous polar plot format (radial lines denote advection time scale in 90 day intervals; points on the clock-face denote months of the year). The spiralling nature of the line shows how the temperature maxima occurs later as the travel time from the Irminger Basin increases.

heating. We then released these particles on 2 September 2000 and tracked them for 15 months. Particles swiftly entered, circumnavigated, and left the Labrador Sea. Consistent with observations and previous model studies [*Lilly et al.*, 2003; *Chanut et al.*, 2008], Cape Desolation (48° W, 60° N) was a favored location for eddying departures from this direct route. About 3% of the particles continued through the Davis Strait into Baffin Bay along the West Greenland coast. We repeated the analysis for years 2001–2009, and these trajectories were related to the spatial variability of the phase in the annual cycle of WL temperature. For each time step we relate the travel time of the particle from the Irminger Basin to the seasonal cycle at that grid point and, in particular, to the month in which the maximum temperature occurs. Figures 4c and 4d show how the month in which the maximum temperature occurs is related to the particle travel time from the Irminger Sea. (We note that this is only relevant to regions downstream of the Irminger Sea, so that other processes must determine seasonal variability in and to the north of the Denmark Strait.) There is a clear indication that the longer the transit time from the Irminger Sea, the later the seasonal temperature maximum is reached. That is, the phase of the WL temperature maximum reflects the time that has elapsed since the parcel of water last reached its seasonal maximum at the surface. Although we emphasize that more winter sub-surface observations are needed to fully constrain the annual cycle of the WL and to examine other processes that might be involved, our current explanation is consistent with both our model analysis and the available observations.

4. Summary and Conclusions

A unique set of observations has been used to improve our description of the sub-surface seasonal cycle of water masses around Greenland between 2002 and 2011. The analysis shows a sub-surface temperature

maximum associated with the coastal boundary current that has a significant seasonal cycle, with a magnitude of the order 1–2°C. In context, this is similar in magnitude to the 1.6°C increase in spring and summer temperatures between 1995 and 1997 for this layer near Disko Bay, in West Greenland [*Holland et al*., 2008; *Hansen et al*., 2012]. This interannual change is thought to have played a significant role in accelerating the melt of Jakobshavn Isbræ outlet glacier. Attempts to quantify the relationship between ocean temperature and glacier melt have yielded a range of results. However, a conservative example suggests that a 1°C temperature increase would be associated with at least a doubling of the ice-melt rate [see *Holland et al*., 2009]. We emphasize, that our analysis does not directly address the extent that the seasonally varying warm layer accesses outlet glaciers to reach the Greenland Ice Sheet, as this question will depend on fjord-specific processes [e.g., *Inall et al*., 2014; *Sutherland and Straneo*, 2012; *Johnson et al*., 2011]. However, as a point of reference, a rare "winter" profile in the vicinity of Helheim Glacier (south-east Greenland) recorded WL temperatures that were 1° warmer in March 2010 than the previous summer (August–September 2009) [*Straneo et al*., 2012]. It is unclear if these summer-winter differences were due to interannual, or seasonal variability [*Straneo et al*., 2012]. Nonetheless, the magnitude of the seasonal temperature range found here implies that it would be important for any assessment of interannual WL changes to take into account the time of year at which observations were obtained.

There is considerable spatial variability in the phase of the WL seasonal cycle around Greenland. In particular, the annual peak in the WL temperature occurs significantly later to the north along the west coast. Particle tracking analysis in a high-resolution ocean model suggests that this spatial variability is determined by the travel time of water from the subduction sites in the Irminger Basin.

Finally, in addition to a significant seasonal temperature range, our results suggest that in some regions the WL may often be warmest in winter, i.e., the most poorly observed period of the year. A recent study of two Greenland fjords suggested that this is also the time of year when fjord-shelf exchanges allow warm subsurface ocean waters to most strongly influence glacier melt rate [*Jackson et al*. 2014]. This highlights the need for year-round subsurface temperature measurements, for a complete description of the WL seasonality, and in particular to ensure that the ice-melting potential of the WL is not underestimated.

Acknowledgments

We acknowledge the use of data from the World Ocean data base (http://www.nodc.noaa.gov/OC5/SELECT/dbsearch/dbsearch.html) and the International Argo program (http://www.usgodai.org/cgi-bin/argo_select.pl). This research was funded by the UK Natural Environment Research Council Grant. NE/H01103X/1. The Canadian marine mammal deployments were funded by Fisheries and Oceans Canada Centre of Expertise in Marine Mammalogy (CEMAM), DFO's International Governance and Atlantic Seal Research Programs, Canada's International Polar Year Program, and the Greenland Institute of Natural Resources. Enquiries about these data should be made to GS (Garry.Stenson@dfo-mpo.gc.ca). The narwhal data were funded by a NOAA Ocean Exploration grant and the Greenland Institute of Natural Resources. Enquiries about this data should be made to KL (klaidre@apl.washington.edu). The Norwegian hooded seal deployments were undertaken within the Norwegian Research Council, International Polar Year project MEOP (Marine Mammals Exploring the Ocean Pole to Pole). Enquiries about this data should be made to KK (kit.kovacs@npolar.no). The high-resolution model runs were supported by NERC National Capability funds and performed on the ARCHER UK National Supercomputing Service.

The Editor thanks two anonymous reviewers for their assistance in evaluating this paper.

References

Andersen, J. M., Y. F. Wiersma, G. Stenson, M. O. Hammill, and A. Rosing-Asvid (2009), Movement patterns of Hooded Seals (*Cystophora cristata*) in the Northwest Atlantic Ocean during the Post-Moult and Pre-Breed seasons, *J. Northw. Atl. Fish Sci.*, *42*, 1–11, doi:10.2960/J.v42.

Andersen, J. M., et al. (2013), Investigating annual diving behaviour by Hooded Seals (*Cystophora cristata*) within the Northwest Atlantic Ocean, *PLoS One*, *8*(11), e80438, doi:10.1371/journal.pone.0080438.

Bailleul, F., V. Lesage, M. Power, D. W. Doidge, and M. O. Hammill (2012), Environmental response in fall migration phenology of beluga in a changing Arctic, *Clim. Res.*, *53*, 169–178.

Barnier, B., et al. (2006), Impact of partial steps and momentum advection schemes in a global ocean circulation model at eddy permitting resolution, *Ocean Dyn.*, *56*, 543–567, doi:10.1007/s10236-006-0082-1.

Blanke, B., and S. Raynaud (1997), Kinematics of the Pacific Equatorial Undercurrent: A Eulerian and Lagrangian approach from GCM results, *J. Phys. Oceanogr.*, *27*, 1038–1053.

Boehme, L., and U. Send (2005), Objective analyses of hydrographic data for referencing profiling float salinities in highly variable environments, *Deep Sea Res., Part II*, *52*, 651–664.

Boehme, L., M. P. Meredith, S. E. Thorpe, M. Biuw, and M. Fedak (2008a), Antarctic Circumpolar Current frontal system in the South Atlantic: Monitoring using merged Argo and animal-borne sensor data, *J. Geophys. Res.*, *113*, C09012, doi:10.1029/2007JC004647.

Boehme, L., S. E. Thorpe, M. Biuw, M. Fedak, and M. P. Meredith (2008b), Monitoring Drake Passage with elephant seals: Frontal structures and snapshots of transport, *Limnol. Oceanogr.*, *53*, 2350–2360.

Boyer, T. P., et al. (2013), World Ocean Database 2013, *NOAA Atlas NESDIS 72*, edited by S. Levitus, 209, pp., Silver Spring, Md.

Chanut, J., et al. (2008), Mesoscale eddies in the Labrador Sea and their contribution to convection and restratification, *J. Phys. Oceanogr.*, *38*, 1617–1643.

Charrassin, J.-B., et al. (2008), Southern Ocean frontal structure and sea-ice formation rates revealed by elephant seals, *Proc. Natl. Acad. Sci. U.S.A.*, *105*, 11,634–11,639, doi:10.1073/pnas.0800790105.

DRAKKAR Group (2007), Eddy-permitting Ocean Circulation Hindcasts of past decades, *CLIVAR Exchanges*, no. 42, *12*(3), 8–10.

Duchez, A., E. Frajka-Williams, N. Castro, J. Hirschi, and A. Coward (2014), Seasonal to interannual variability in density around the Canary Islands and their influence on the Atlantic meridional overturning circulation at 26°N, *J. Geophys. Res. Oceans*, *119*, 1843–1860, doi:10.1002/2013JC009416.

Fratantoni, P. S., and R. S. Pickart (2007), The Western North Atlantic shelfbreak current system in summer, *J. Phys. Oceanogr.*, *37*, 2509–2533, doi:10.1175/JPO3123.1.

Grist, J. P., S. A. Josey, L. Boehme, M. P. Meredith, F. J. M. Davidson, G. B. Stenson, and M. O. Hammill (2011), Temperature signature of high latitude Atlantic boundary currents revealed by marine mammal-borne sensor and Argo data, *Geophys. Res. Lett.*, *38*, L15601, doi:10.1029/2011GL048204.

Hansen, M. O., T. G. Nielson, C. A. Stedmon, and P. Munk (2012), Oceanographic regime shift during 1997 in Disko Bay, Western Greenland, *Limnol. Oceanogr.*, *57*, 634–644, doi:10.4219/lo.2012.57.2.0634.

Hecht, M. W., and R. D. Smith (2013), Toward a physical understanding of the North Atlantic: A review of model studies in an eddying regime, *Geophys. Monogr. Ser.*, *177*, 213–239.
Holland, D. M., R. H. Thomas, B. de Young, M. Ribergaard, and B. Lyberth (2008), Acceleration of Jakobshavn Isbræ triggered by warm subsurface ocean waters, *Nat. Geosci.*, *1*, 659–664.
Holland, P. R., A. Jenkins, and D. M. Holland (2009), The response of ice shelf basal melting to variations in ocean temperature, *J. Clim.*, *21*, 2558–2572.
Inall, M. E., et al. (2014), Oceanic heat delivery via Kangerdlugssuaq Fjord to the south-east Greenland ice sheet, *J. Geophys Res. Oceans*, *119*, 631–645, doi:10.1002/2013JC009295.
Ingleby, B., and M. Huddleson (2007), Quality control of ocean temperature and salinity profiles-historical and real-time data, *J. Mar. Syst.*, *65*, 158–175, doi:10.1016/j.jmarsys.2005.11.019.
Isachsen, P. E., S. R. Sørlie, C. Mauritzen, C. Lydersen, P. Dodd, and K. M. Kovacs (2014), Upper-ocean hydrography of the Nordic Seas during the International Polar Year (2007-2008) as observed by instrumented seals and Argo floats, *Deep Sea Res., Part I*, *93*, 41–59, doi:10.1016/j.dsr.2014.06.012.
Jackson, R. H., F. Straneo, and D. A. Sutherland (2014), Externally forced fluctuations in ocean temperature at Greenland glaciers in non-summer months, *Nat. Geosci.*, doi:10.1038/NGEO2186.
Johnson, H. L., A. Munchow, K. K. Falkner, and H. Melling (2011), Ocean circulation and properties in Petermann Fjord, Greenland, *J. Geophys. Res.*, *116*, C01003, doi:10.1029/2010JC006519.
Jutzeler, M., et al. (2014), On the fate of pumice rafts formed during the 2012 Havre submarine eruption, *Nat. Commun.*, *5*, 3660, doi:10.1038/ncomms4660.
Laidre, K. L., M. P. Heide-Jørgensen, W. Ermold, and M. Steele (2010), Narwhals document continued warming of southern Baffin Bay, *J. Geophys. Res.*, *115*, C10049, doi:10.1029/2009JC005820.
Levitus, S., J. I. Antonov, T. P. Boyer, R. A. Locarnini, H. E. Garcia, and A. V. Mishonov (2009), Global ocean heat content 1955-2008 in light of recently revealed instrumentation problems, *Geophys. Res. Lett.*, *36*, L07608, doi:10.1029/2008GL037155.
Lilly, J. M., P. B. Rhines, F. Schott, K. Lavender, J. Lazier, U. Send, and E. D'Asaro (2003), Observations of the Labrador Sea eddy field, *Prog. Oceanogr.*, *59*, 75–176.
Madec, G. (2008), NEMO Ocean Engine, Note du pôle modélisation 27, Institut Peirre-Simon Laplace (IPSL).
Mauritzen, C. (1996), Production of dense overflow waters feeding the North Atlantic across the Greenland-Scotland Ridge. Part 1: Evidence for a revised circulation scheme, *Deep Sea Res., Part II*, *43*, 769–806.
Meredith, M. P., K. W. Nicholls, I. A. Renfrew, L. Boehme, M. Biuw, and M. Fedak (2011), Seasonal evolution of the upper-ocean adjacent to the South Orkney Islands, Southern Ocean: Results from a 'lazy biological mooring', *Deep Sea Res., Part II*, *58*, 1569–1579.
Mortensen, J., K. Lennert, J. Bendtsen, and S. Rysgaard (2011), Heat sources for glacial melt in a sub-Arctic Fjord (Godthadsfjord) in contact with the Greenland Ice Sheet, *J. Geophys. Res.*, *116*, C01013, doi:10.1029/2010JC006528.
Myers, P. G., and M. H. Ribergaard (2013), Warming of the Polar Water Layer in Disko Bay and potential impact on Jakobshavn Isbræ, *J. Phys. Oceanogr.*, *43*, 2629–2640, doi:10.1175/JPO-D-12-051.1.
Roquet, F., et al. (2013), Estimates of the Southern Ocean general circulation improved by animal-borne instruments, *Geophys. Res. Lett.*, *40*, 6176–6180, doi:10.1002/2013GL058304.
Straneo, F., G. S. Hamilton, D. A. Sutherland, L. A. Stearns, F. Davidson, M. O. Hammill, G. B. Stenson, and A. Rosing-Asvid (2010), Rapid circulation of warm subtropical waters in a major glacial fjord in East Greenland, *Nat. Geosci.*, *3*, 182–186, doi:10.1038/NGEO764.
Straneo, F., D. A. Sutherland, D. Holland, C. Gladish, G. S. Hamilton, H. L. Johnson, E. Rignot, Y. Xu, and M. Koppes (2012), Characteristics of ocean waters reaching Greenland's glaciers, *Ann. Glaciol.*, *53*(60), doi:10.3189/2012AoG60A059.
Sutherland, D. A., and F. Straneo (2012), Estimating ocean heat transports and submarine melt rates in Sermilik Fjord, Greenland, using lowered acoustic Doppler current profiler (LADCP) velocity, *Ann. Glaciol.*, *53*, 50–58.
Sutherland, D. A., F. Straneo, G. B. Stenson, F. J. M. Davidson, M. O. Hammill, and A. Rosing-Asvid (2013), Atlantic water variability on the SE Greenland continental shelf and its relationship to SST and bathymetry, *J. Geophys. Res. Oceans*, *118*, 847–855, doi:10.1029/2012JC008354.
Tang, C. C. L., C. K. Ross, T. Yao, B. Petrie, B. M. DeTracey, and E. Dunlap (2004), The circulation, water masses and sea-ice of Baffin Bay, *Progr. Oceanogr.*, *63*, 183–228, doi:10.1016/j.pocean.2004.09.005.
Zhu, J., and E. Demirov (2011), On the mechanism of interannual variability of the Irminger water in the Labrador Sea, *J. Geophys. Res.*, *116*, C03014, doi:10.1039/2009JC005677.